JOURNAL OF OPTOELECTRONICS AND ADVANCED MARERIALS Vol. 9, No. 6, June 2007, p. 1750 - 1756

Point defects and oxygen diffusion in fluorite type oxides

P. CRISTEA*, M. STAN[a], J. C. RAMIREZ[a]
University of Bucharest – Faculty of Physics, Bucharest-Măgurele, Romania
[a]os Alamos National Laboratory, Los Alamos, NM 87545, USA

We present thermodynamic models of point defects formation in fluorite-type oxides with important technological applications, such as hypostoichiometric ceria CeO_{2-x} and plutonia PuO_{2-x}. The concentrations of defect species were calculated at different temperatures and partial pressures of oxygen. To highlight some of the current capabilities of the approach, a number of example applications, including the calculation of defect configuration entropy, and the calculation of self and chemical diffusivities of oxygen as a function of nonstoichiometry and temperature are addressed. The results provided by the modeling are validated against available experimental data on non-stoichiometry and oxygen diffusivity.

(Received November 14, 2006; accepted April 26, 2007)

Keywords: Point defects, Diffusion, Nuclear fuels

1. Introduction

Understanding the structure and the properties of defect lattices is of paramount importance in materials science, since the atomistic mechanisms control the bulk transport phenomena. In most cases, at high temperature, the defect-related behavior of quasi-pure materials is dominated by the point defects. Moreover, due to their low dimensionality associated with high configurational entropy, these are the only defects that can exist in a thermodynamic equilibrium state. Roughly, the concentration of point defects increases with the temperature and the departure from stoichiometry, and decreases with pressure [1]. A striking fact related to the behavior of point defects is the recent discovery of a simple, but universal, correlation between the symmetry of short-range order (SRO) distribution of point defects and crystal symmetry [2].

There are three important thermodynamic quantities associated with the formation of point defects in a crystal: the energy of formation, the entropy of formation and the elastic dipole tensor. Of these, the best understood and the easiest to calculate is the energy of formation. The traditional mass action law is widely used to calculate the concentration of lattice defects. This formalism assumes that the defects do not interact, and that each defect occupies only one lattice site. However, complex defect structures occupy many sites, and the strong Coulomb and elastic repulsions may exclude other complexes from nearby sites. This is a source of great complications in any statistical description, especially when the defect complexes are anisotropic [3]. The effect of defect interaction is sometimes the driving force behind the segregation of a new phase and a lot of attention has been focused on the deficiencies of the mass action formalism at high defect concentration. Consequently, improved methods were introduced to determine the distribution of the defects [4].

The diffusivity is one of the key theoretical parameters in understanding the crystal growth and the microstructure evolution under different environmental conditions. Properly speaking, modeling of diffusivity involves concepts and methods belonging to non-equilibrium thermodynamics.

The basic events involved in migration processes are represented as the discrete hops of various atoms. In most lattices, the hopping species are defects and the rate of diffusion is basically controlled by the concentrations and jump frequencies of these defects. Understanding experimental data in the light of such a representation is not always an easy task. Usually, the application of absolute rate theory to diffusive jumps requires the existence of a transition state with a lifetime sufficiently long for the thermodynamic properties of the jumping atom to be defined. The existence of a thermodynamically activated state requires experimental validation. However, as noticed by Rice [5], there is some consensus that, in most cases, the diffusing species spends most of its time on one or the other side of the barrier and the crossing barrier process is a very fast one. Therefore, the existence of an activated state is probably an oversimplification. Maier et al. [6] advanced interesting ideas regarding the kinetics of oxygen incorporation in oxides, the impact of bulk diffusion, surface reaction, and grain boundaries.

Surprisingly, despite they are persistently studied for their importance in the nuclear fuels technology, what is less known about UO_2, or other actinide oxides, is that they are also receiving great attention for prospective use in electronic devices. Semiconductors that are based on uranium dioxide (or other actinide compounds) could offer significant improvements in performance as compared to conventional Si, Ge, and GaAs materials. The energy band gap for uranium dioxide lies between Si and GaAs at the optimum of the band gap vs. efficiency curve, indicating that one should be able to use uranium oxides to make

very efficient solar cells, semiconductors, or other electronic devices [7].

The purpose of the present paper is to present simple and efficient models of defect species and of oxygen diffusion in two famous fluorite-structured metal oxides, namely the hypostoichiometric ceria CeO_{2-x} and hypostoichiometric plutonia PuO_{2-x}. The paper analyzes the role played by some possible diffusion-mediated interactions between various point defects. The consequences and the applications of these models to calculate the oxygen self and chemical diffusivities are briefly discussed.

2. Modeling

2.1 Background

Pure stoichiometric fluorite-structured metal oxides MO_2 have four metal atoms (M) and eight oxygen atoms (O) per unit cell, and the space group *Fm-3m* (Fig. 1). Each oxygen atom resides in the centre of a tetrahedron having four metal atoms in the apexes.

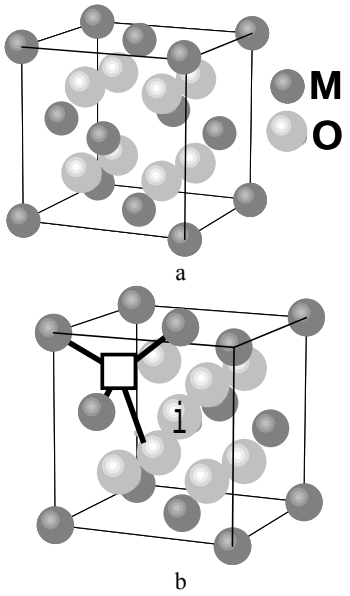

Fig. 1. a) Lattice unit cell for the stoichiometric MO_2 fluorite oxides. The generic metal atom (M) plays the role of Ce, Pu, or U atoms. b) Two of the most frequent encountered point defect species: the oxygen vacancy V_O (CeO_{2-x}, PuO_{2-x}), and the oxygen interstitial O_i (UO_{2+x}).

The oxygen sublattice is simple cubic, with each oxygen atom surrounded by six nearest O neighbours. All studied oxides have almost the same lattice parameter *a*: 5.411 Å for ceria [8], 5.396 Å for plutonia, and 5.47 Å for urania [9].

An introduction to the physical and chemical properties of pure and doped ceria, commonly used as a surrogate to predict the properties of plutonium oxides, is available in a review by Mogensen [10]. Both CeO_2 and PuO_2 lattices accommodate an extensive hypostoichiometry, this behaviour being associated with the production of oxygen vacancies in the oxygen sublattice, and the ease of reduction of metal ions Ce^{4+} and Pu^{4+} ions to Ce^{3+} and respectively to Pu^{3+}. Ce^{3+} ions represent electronic states trapped at some cerium sites, surrounded by the lattice polarization that they induce (small polarons). This proved to be a reasonable description of CeO_{2-x} [11]. Recently, carefully conducted quantum mechanics calculations revealed that a similar behaviour of Pu^{3+} ions may exists in PuO_{2-x} [12].

Although the UO_2 oxide adopts the same fluorite structure, the process of reduction of U^{4+} to U^{3+} requires significantly more energy, with the result that the hypostoichiometry can only be measurable at very high temperatures and very low partial pressures of oxygen. In UO_{2+x}, a facile valence change U^{4+} to U^{5+} replaces the reduction of metal ions, a mechanism that leads to a wide range of hyperstoichiometry, up to at least $UO_{2.3}$. As first shown by neutron diffraction studies [13], the excess oxygen ions are incorporated at interstitial sites (Fig.1). Such a different behaviour indicates that not solely the lattice symmetry is involved in the details of evolution toward thermodynamic equilibrium with a given surrounding oxygen atmosphere. The nature, the strength, and the fine details of complex interactions of constituent atoms also play an important role.

Throughout this paper the defects are indicated in the Kröger-Vink convention [14, 15].

2.2 Point defects and oxygen diffusion in CeO_{2-x} and PuO_{2-x} (M ≡ Ce, or Pu)

Based on experimentally observed similarities in the behavior of CeO_{2-x} and PuO_{2-x}, a model similar to [4] was recently used [16, 17] to evaluate the thermodynamic properties of PuO_{2-x}. For both ceria and plutonia, five types ($\alpha = 1 \div 5$) of defect species were included: small polarons $M_M^{/}$, singly and doubly positively charged oxygen vacancies $V_O^{\bullet}$ and $V_O^{\bullet\bullet}$, singly positively charged defect pairs $(MV_O)^{\bullet}$, and neutral defect pairs $(MV_O)^{\times}$.

As experimentally confirmed, the cation (M ≡ Ce, or Pu) mobility is negligible when compared to the mobility of oxygen [18]. The oxygen only moves in its simple cubic sublattice and is not able to jump until an oxygen vacancy or a (MV_O) pair arrives at a neighboring site. At low oxygen deficiency *x*, the lattice configurations containing two, or more, oxygen defects residing on nearest neighbor positions around non-defective oxygen sites make an almost insignificant contribution. This approximation restricts the range of nonstoichiometry to $x < 0.17$. This work assumes that the oxygen diffusion in both ceria and plutonia is controlled by a two-channel charge transport mechanism between defective oxygen sites. The first channel is dominated by the jumps of O^{1-} ions, while the second involves the jumps of O^{2-} ions. Bellow, we shall be concerned with determining the channel dominating various ranges of oxygen deficiency.

When an oxygen atom attempts to jump to an empty nearest-neighbor site, its motion is unavoidably affected by the dynamics of local lattice deformation, part of which depends on the orientation of (MV_O) defect pairs relative to the jumping atom. Fig 2 shows that different outcomes are possible as a function of pair orientation.

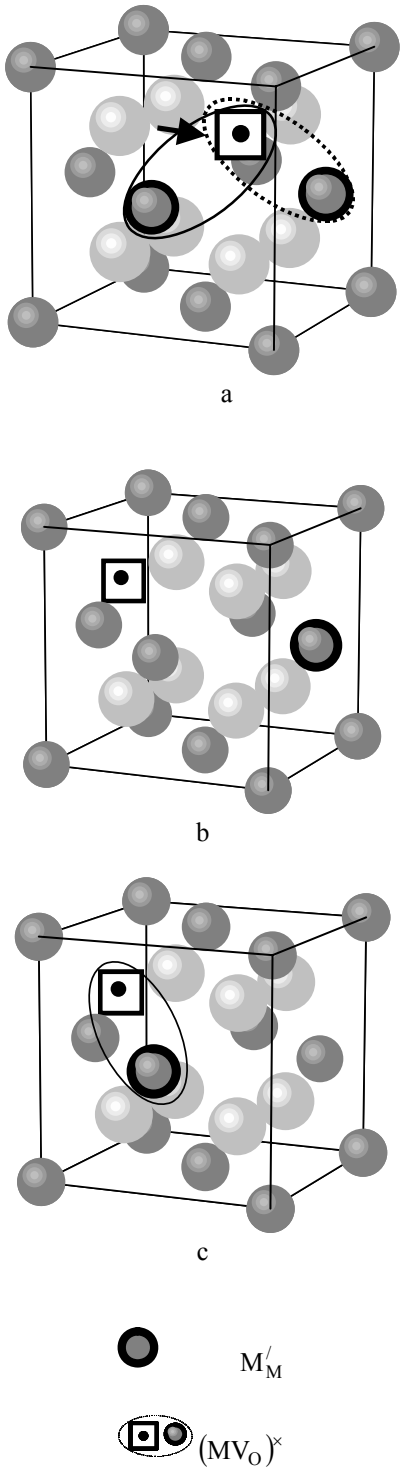

Fig. 2. The outcome caused by an oxygen jump into a vacancy belonging to a $(MV_O)^{\times}$ *pair may depend on the pair orientation. a) The* $(MV_O)^{\times}$ *pair in the full line envelope has its polaron* $M_M^{/}$ *close to the jumping O atom. For the pair in the dash envelope* $M_M^{/}$ *resides far away from the jumping ion. After the jump, the pair in dash envelope dissociates into a* $V_O^{\bullet}$ *vacancy and a polaron* $M_M^{/}$ *(b), while the pair in the full line envelope only changes its orientation (c) [19].*

In addition, we anticipate that the interactions with polarons, followed by the association with oxygen vacancies, can play a significant role in deciding the possible outcomes after a diffusion jump. The formation of composite defects, such as (MV_O) pairs, is equivalent to an interaction correlating the jumps of oxygen ions with the hopping of small polarons. Therefore, as long as this coupling is significant, i.e. the pairs represent the dominant defect species in a given nonstoichiometry range, we expect for the mobility of oxygen to be coupled to that of small polarons $M_M^{/}$. The change in identity of defect species during diffusion jumps can, to some extent, be interpreted as *diffusion-mediated interactions*. Below, we used the handy notation $\langle \alpha, O^n \rangle$ to indicate that oxygen ion jumps into an α defect site and behaves as an O^n ion ($n = -1,-2$). Such a process is represented as

$$\langle \alpha, O^n \rangle \rightarrow \beta \oplus (...) \qquad (1)$$

Here, β describes the resulting oxygen defect species after the jump, the operator $\oplus$ is meant to show that no further association ("reaction") is involved between the operands, and (…) stands for other possible non-oxygen defects (i.e., polarons). The new local configuration acts as initial configuration for the next jump, and so on. For consistency with the previous assumptions, all new configurations containing more than one oxygen defect among the nearest neighbors were ignored.

The possible values of β were analyzed for all possible combinations of α and n, and the outcomes are listed in Table 1.

Table 1. Outcome configurations β *generated by the jumps* $\langle \alpha, O^n \rangle$ *of* O^n *ions to* α*-type defect sites.*

	α	Final configurations	
		Jumping ion: O^{-1}	Jumping ion: O^{-2}
Initial configuration	$V_O^{\bullet}$	$V_O^{\bullet}$, $(MV_O)^{\times}$	$V_O^{\bullet\bullet} \otimes M_M^{/}$, $(MV_O)^{\bullet}$
	$V_O^{\bullet\bullet}$	$V_O^{\bullet}$, $(MV_O)^{\times}$	$V_O^{\bullet\bullet}$, $(MV_O)^{\bullet}$
	$(MV_O)^{\bullet}$	$V_O^{\bullet}$, $(MV_O)^{\times}$	$V_O^{\bullet\bullet} \otimes M_M^{/}$, $(MV_O)^{\bullet}$
	$(MV_O)^{\times}$	$V_O^{\bullet} \otimes M_M^{/}$, $(MV_O)^{\times}$	$V_O^{\bullet\bullet} \otimes 2M_M^{/}$, $(MV_O)^{\bullet} \otimes M_M^{/}$

The results show that the jumps of O^{1-} ions mainly generate $V_O^{\bullet}$ and $(MV_O)^{\times}$ defect species. This situation strongly suggests that the diffusion of oxygen should be controlled by the jumps of O^{1-} oxygen ions when $V_O^{\bullet}$, or

$(MV_O)^{\times}$, species are dominant. In contrast, the jumps of O^{2-} oxygen ions are seen to essentially create $V_O^{\bullet\bullet}$, polarons ($M_M^{/}$), and $(MV_O)^{\bullet}$ only. Therefore, when these species dominate, we expect for the O^{2-} ions to control the diffusion.

A statistical thermodynamic approach, appropriate for the nonstoichiometric case, that uses the equations presented in TABLE II and allows for the calculation of various contributions x_α, was described elsewhere [4, 17].

2.3 Oxygen self and chemical diffusivity

The frequency associated to the jumps of oxygen ions was modeled as a function of x and T using the dependence given in [17, 19, 20]:

$$\nu(x,T) = \nu_0 \exp\left(-\frac{E_m}{k_B T}\right)\exp\left[-\frac{E_f(x,T)}{k_B T}\right]. \quad (2)$$

Here, ν_0 is an effective vibrational frequency, E_m is the average migration energy of oxygen, and $E_f(x,T)$ is the average formation energy of defective oxygen sites:

$$E_f(x,T) = k_B T \sum_\alpha (x_\alpha / x)\ln(2/x_\alpha). \quad (3)$$

Typically, the prefactor ν_0 is on the order of 10^{13} s^{-1}. Using Eqn. (2), the self-diffusivity, $D_s(x,T)$ is calculated using the general form [17, 19]:

$$D_s(x,T) = (a_o^2/24) f_{av}(x)\nu(x,T). \quad (4)$$

In this equation, a_0 is the lattice constant, and $f_{av}(x)$ is the average correlation factor, constructed using the correlation factors $f(x_\alpha)$ of individual species [17, 19]:

$$f_{av}(x) = (1/x)\sum_\alpha x_\alpha f(x_\alpha). \quad (5)$$

The expression of $f(x_\alpha)$ in Eqn. (5) was adapted to the present case from literature [21-23]:

$$f(x_\alpha) = \frac{(2+x_\alpha)f_0}{(2f_0 - 1)x_\alpha + 2}, \quad (6)$$

where $f_0 = 0.653$ is the correlation factor in a simple cubic lattice [24].

When the diffusion occurs under a chemical concentration gradient, the chemical diffusivity $D_c(x,T)$ should be used instead of self-diffusivity. Important examples include the inter-diffusion of two materials, chemical doping of semiconductors, and the situations where the stoichiometry of the material changes as a result of a change in the defects concentration. The chemical diffusivity can be calculated as a function of x and T from self-diffusivity, by dividing Eqn. (4) with the correlation factor $f_{av}(x)$, and multiplying it with the thermodynamic factor [25]:

$$D_c(x,T) = D_s(x,T)\frac{1}{f_{ax}(x)}\frac{d\ln a_O}{d\ln[O]} = D_s(x,T)\frac{1}{f_{ax}(x)}\left(1+\frac{d\ln\gamma_O}{d\ln[O]}\right), \quad (7)$$

where the chemical activity of oxygen a_O, in a given nonstoichiometric oxide in equilibrium with the environment, is given by $\ln a_O = \Delta G_{O_2}(x,T)/2RT$ [18], and γ_O is the activity coefficient of oxygen. In the partial excess Gibbs energy of oxygen $\Delta G_{O_2} = RT\ln P_{O_2}$, the dimensionless partial pressure of oxygen P_{O_2} is measured with respect to the normal pressure. The atomic fraction of oxygen [O], in a nonstoichiometric oxide $MO_{2\pm x}$, is $[O] = (2\pm x)/(3\pm x)$. Therefore, $d\ln[O] = \pm dx/(x\pm 2)(x\pm 3)$. As a result, the chemical diffusion coefficient for a $MO_{2\pm x}$ oxide is given by:

$$D_c(x,T) = D_s(x,T)\frac{\pm(x\pm 2)(x\pm 3)}{2RTf_{av}(x)}\frac{d}{dx}\left(\Delta G_{O_2}\right). \quad (8)$$

The + sign should be used in the hyperstoichiometric case, while the – sign holds for the hypostoichiometric case. The result was recently used in [17] to calculate the chemical diffusivity of PuO_{2-x}.

3. Results

We focused our attention on the symbolic defect equations supporting the formation of point defects presented in Section 2.2. Several possible paths are listed in TABLE II. The statistical thermodynamic approach [4, 17] was incorporated in a Mathcad simulation program and applied to analyze the thermodynamic behavior of CeO_{2-x} and PuO_{2-x},. Using as a trial parameters the enthalpies and the entropies associated to the quasi-chemical equations describing the formation of defect species listed in TABLE II, the concentrations of defect species were determined with the conjugate-gradient method. Consequently, the values were continuously optimized until a self-consistent good agreement with the reported experimental dependencies of nonstoichiometry x in MO_{2-x} on temperature and partial pressure of oxygen was observed. The optimized values were consequently used to predict the defect species concentration and the nonstoichiometry as a function of oxygen pressure in a different temperature range. Afterward, the concentration of various defect species x_α, as measured with respect to the concentration of cation sites, was calculated using the ratio N_α / N_C, with N_α the total number of α-type defects, and N_C the number of cationic sites in the lattice (N_A/N_C=2).

Table 2. The enthalpies and entropies parameters associated to the defect reactions used in the present calculation of defect species concentration.

	Defect Reaction	M ≡ Ce		M ≡ Pu	
		h (eV)	s (k_B)	h (eV)[c]	s (k_B)[c]
CeO_{2-x} and PuO_{2-x}	$O_O^{\times} + 2M_M^{\times} \leftrightarrow (1/2)O_2 + V_O^{\bullet\bullet} + 2M_M^{/}$	4.90[a,d] 5.0[b]	16.129[a,d] 16.732[b]	4.8	6.382
	$V_O^{\bullet} + M_M^{\times} \leftrightarrow V_O^{\bullet\bullet} + M_M^{/}$	0.16[a,d] 0.17[b]	- 3.446[a,d] - 3.573[b]	0.2	- 2.901
	$M_M^{/} + V_O^{\bullet\bullet} \leftrightarrow (MV_O)^{\bullet}$	- 0.25[a,d] - 0.25[b]	0[a,d] 0[b]	- 0.1	0
	$M_M^{/} + V_O^{\bullet} \leftrightarrow (MV_O)^{\times}$	- 0.15[a,d] - 0.15[b]	0.812[a,d] 0.793[b]	- 0.3	0

[a] This work. [b] [4] . [c] [17]. [d] [19].

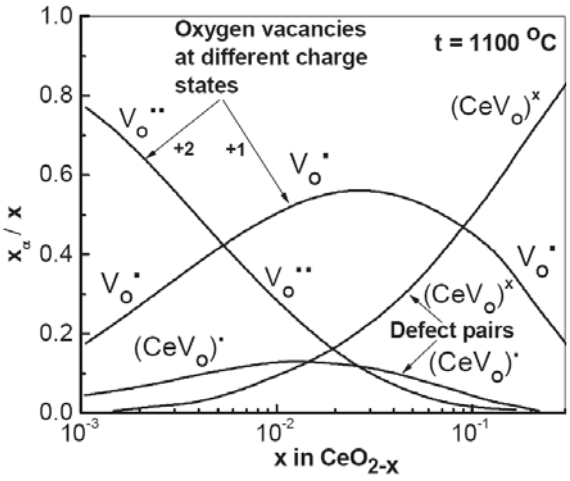

a

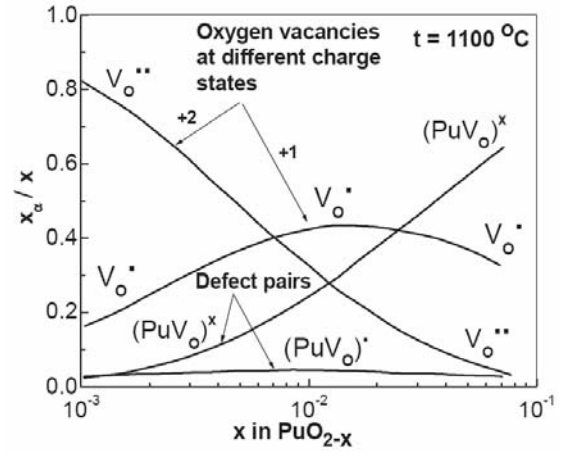

b

Fig. 3. Calculated relative contributions to non-stoichiometry x_α / x, $\alpha = 1 \div 4$, in CeO_{2-x} and PuO_{2-x}.

Figs. 3(a, b) show the calculated relative contributions x_α / x of different defect species to nonstoichiometry in CeO_{2-x} and PuO_{2-x}. The curves look very similar, and in both cases the nearly stoichiometric region is dominated by $V_O^{\bullet\bullet}$ and $M_M^{/}$. However, the $V_O^{\bullet}$ vacancies dominate the intermediate range, while in the highly nonstoichiometric region the neutral pairs $(MV_O)^{\times}$ take over. When corroborated with the findings shown in TABLE I, the calculation shows that, according to our model, in the nearly stoichiometric ceria and plutonia, the diffusion of oxygen is primarily controlled by O^{2-} ions, while in the intermediate and in the highly nonstoichiometric region the O^{1-} ions takes over. Also, for highly nonstoichiometric oxides, the jumps of oxygen atoms are correlated with the hopping polarons in the cation sublattice. Since, usually, we expect for the polarons to have a higher mobility, such a coupling will introduce a tendency to saturation in the mobility of O ions, and an increase in the activation energy of the polaron hopping process.

As can be seen in Fig.4 (a,b), despite their almost identical behavior as functions of nonstoichiometry (Fig. 4a), the defect configurational entropies (per cationic site) for ceria and plutonia look very different when compared at the same temperature and partial pressure of oxygen. This is due to the different defect formation enthalpies and entropies, as shown in TABLE II. However, we observed that the behavior of defect configurational entropy as a function of oxygen deficiency x, is an almost universal function, given by:

$$s_c = s_{c,0} x^{\gamma} \tag{9}$$

where $s_{c,0} \cong 3.2 k_B$, and $\gamma \cong 0.63$. The justification of such a behavior is beyond the purpose of this paper.

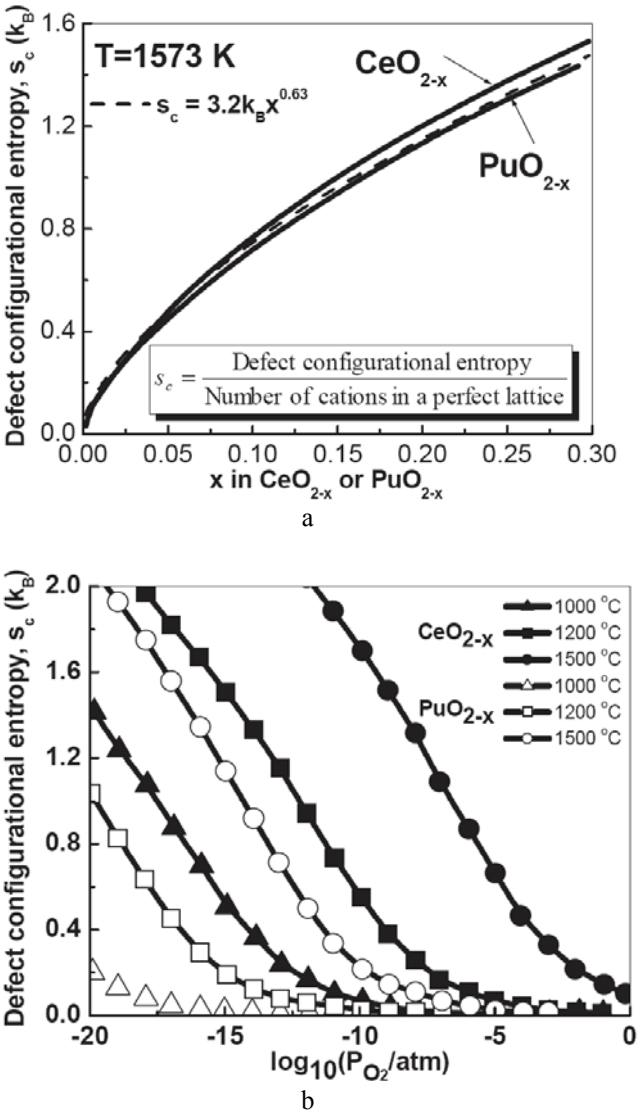

Fig. 4. Comparison of calculated (this work) defect configurational entropy in ceria and plutonia as a function of nonstoichiometry (a), and as a function of partial pressure of oxygen. The partial pressure of oxygen is measured relative to the normal pressure.

Fig. 5(a, b) show the calculated self-diffusivity in CeO_{2-x} and PuO_{2-x}. Despite their simplicity and of some rough assumptions, the models are seen to predict diffusivities in a surprisingly close agreement with the experimental results. Since, at this time, the main goal of the models was to relate atomic scale properties of defects to macroscopic oxygen diffusion, we consider this qualitative agreement as satisfactory. We trust that, provided better values of the free energy of formation of different defect types, the agreement with experimental data and the predictive character of the model will improve.

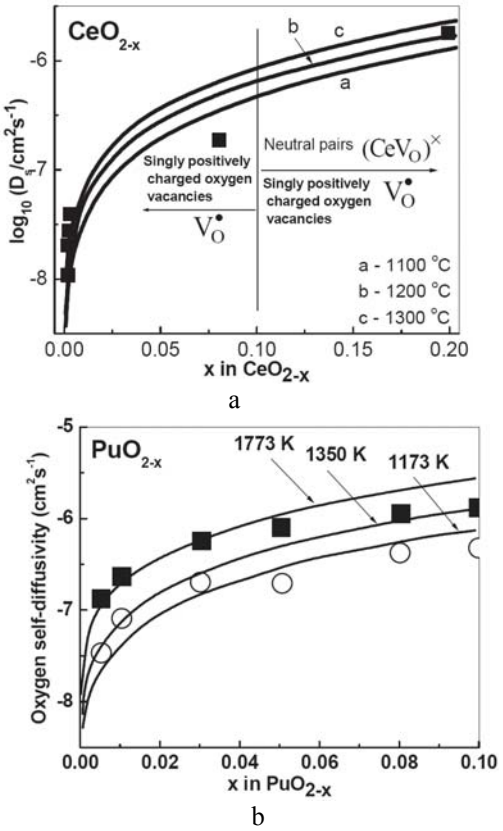

Fig. 5. Oxygen self-diffusivity in CeO_{2-x} (a) and PuO_{2-x} (b) as a function of nonstoichiometry. a) Full line: calculated with Eqn. (4), and $\nu_0 = 3\times10^{13}\ s^{-1}$, $E_m = 0.55$ eV [19]. Black squares: experimental data [26]. b) Full line: calculated with Eqn. (4) using $\nu_0 = 3\times10^{13}\ s^{-1}$ and $E_m = 0.45$ eV [17]. Symbols: data for T = 1350 K; black squares – theoretically evaluated using experimental data obtained provided by the dilatometry method; circles – theoretically evaluated using the thermogravimetric method [27].

4. Conclusions

We used a statistical thermodynamic approach to calculate the nonstoichiometry, the defect configurational entropy, and the diffusivity of oxygen in fluorite type structured ceria and plutonia. Based on the corresponding equations for diffusion-mediated interactions in ceria and plutonia, the outcome configurations caused by the jumps of oxygen ions O^{-1}, O^{-2} have been derived. Such a description was subsequently combined with the numerical results of defect thermochemistry calculations, and related to the charge carried by the oxygen ions during diffusion jumps. Accordingly, in ceria and plutonia, we found that close to the stoichiometric region, the diffusion mediated by O^{2-} ions dominates, while in the deep nonstoichiometry region the O^{1-} ions seem to play the main role. A simple model of oxygen diffusivity was described, and its predictions were compared to the experimental data. The comparison shows a reasonable good agreement with the measured self and chemical diffusivities. Still, a lot of progress is needed to accurately describe the probably

complex defect structure of these materials. However, until more elaborate electronic structure calculations will be able to fully describe the high temperature properties of nonstoichiometric oxides, we trust that valuable information can be extracted using the available thermochemical methods.

Acknowledgements

This work was performed under the auspices of DOE-NE, Advanced Fuel Cycle Initiative AFCI, at Los Alamos National Laboratory. We are pleased to thank B. P. Uberuaga, C. Deo, K. McClellan, S. Valone, S. G. Srivilliputhur, C. Stanek, and S. Rudin (Los Alamos National Laboratory, NM, USA) for useful comments and discussions regarding this work. P.C. is grateful to the Los Alamos National Laboratory, for the warm hospitality and for financial support.

References

[1] A. R. Allnatt, A. B. Lidiard, Atomic Transport in Solids. 1993, Cambridge: Cambridge University Press.
[2] X. Ren, K. Otsuka, Phys. Rev. Lett. **85**, 1016, (2000).
[3] J. H. Harding, J. Chem. Soc., Faraday Trans. **2**(83), 1177, (1987).
[4] S. Ling, Phys. Rev. **B 49**, 864, (1994).
[5] S. A. Rice, Phys. Rev. **112**, 804, (1958).
[6] J. Maier, J. Jamnik, M. Leonhardt, Solid State Ionics, Diffusion and Reactions **129**, 25, (2000).
[7] T. Meek, M. Hu, M. J. Haire, in Waste Management Symposium, 2001, Tucson, AZ, USA.
[8] J. R. Sims, R. N. Blumenthal, High Temp. Sci. **8**, 99, (1976).
[9] F. Gronvold, J. Inorganic and Nuclear Chemistry, **1**, 357, (1955).
[10] M. Mogensen, N.M. Sammes, and G.A. Tompsett, Solid State Ionics, Diffusion and Reactions **129**, 63, (2000).
[11] H. L. Tuller, A.S. Nowick, J. Phys. Chem. Solids **38**, 859, (1977).
[12] L. Petit, A. Svane, Z. Szotek, W. M. Temmerman, Science **301**, 498, (2003).
[13] B. T. M. Willis, Solid State Communications **2**, 23, (1964).
[14] F. A. Kröger, H. J. Vink, eds. Solid State Physics: Advances in Research and Applications. ed. F.S.a.D. Turnbull. **3**. Academic, New York: New York. p. 307 (1956).
[15] M. Barsoum, Fundamentals of Ceramics. McGraw-Hill series in materials science and engineering. 1997: McGraw-Hill.
[16] M. Stan, P. Cristea, Trans. Amer. Nucl. Soc **91**, 491, (2004).
[17] M. Stan, P. Cristea, J. Nucl. Mat. **344**, 213, (2005).
[18] H. Matzke, ed. Non-Stoichiometric Oxides, chap.4. ed. O.T. Sorensen. 1981, Academic Press: New York.
[19] P. Cristea, M. Stan, TMS Letters **2**, 91, (2005).
[20] P. Cristea and M. Stan, in Materials Modeling and Simulations for Nuclear Fuels, MMSNF-4 Workshop, 2005, Washington, D.C., USA.
[21] K. Nakazato, K. Kitahara, Prog. Theor. Phys. **64**, 2261, (1980).
[22] R.A. Tahirkheli, Phys. Rev. B **28**, 3049, (1983).
[23] R.A. Tahirkheli and R.J. Elliott, Phys. Rev. B **27**, 844, (1983).
[24] J.R. Manning, Diffusion Kinetics for Atoms in Crystals. 1968: D. Van Nostrand Company, Inc.
[25] D.S. Tannhauser, in Transport in Nonstoichiometric Compounds, 1985: Plenum, New York.
[26] B.C.H. Steele and J.M. Floyd, Proc. British Ceram. Soc. **19**, 55, (1971).
[27] A. S. Bayoglu, R. Lorenzelli, J. Nucl. Mater. **82**, 403, (1979).

*Corresponding author: pcristea@gmail.com